Lepton fluxes from atmospheric charm

L. Pasquali and M. H. Reno
Department of Physics and Astronomy, University of Iowa, Iowa City, Iowa 52242

I. Sarcevic
Department of Physics, University of Arizona, Tucson, Arizona 85721

(Received 17 July 1998; published 11 January 1999)

We reexamine the charm contribution to atmospheric lepton fluxes in the context of perturbative QCD. We include next-to-leading order corrections and discuss theoretical uncertainties due to the extrapolations of the gluon distributions at small x. We show that the charm contribution to the atmospheric muon flux becomes dominant over the conventional contribution from π and K decays at energies of about 10^5 GeV. We compare our fluxes with previous calculations.
[S0556-2821(99)00203-9]

PACS number(s): 96.40.Tv, 12.38.Bx

I. INTRODUCTION

Neutrino and muon fluxes from cosmic ray interactions with the Earth's atmosphere have been topics of considerable experimental and theoretical interest [1]. At energies near 1 GeV, the IMB [2], Kamiokande [3], and Soudan [4] experiments detect an excess of ν_e relative to ν_μ in the atmospheric neutrinos. Recent results from SuperKamiokande [5] appear to confirm this observation. At these energies, the leptonic decays of charged pions and leptonic and semileptonic decays of kaons are responsible for the lepton fluxes, the so-called ''conventional'' lepton flux. Currently, it is believed that the conventional flux dominates until energies of about 10^3 TeV, when the effects of atmospheric charm production and decay become important contributions to the lepton fluxes. The issue of where the charm contributions dominate is of interest, in part, because this is an energy regime accessible to large underground experiments [6]. Recent results from Fréjus [7], Baksan [8], and other experiments [9] show an excess relative to the conventional muon flux in the 10 TeV energy range. This may be an indication of a charm contribution at lower energies than expected. One of the main goals of the neutrino experiments such as the Antarctic Muon and Neutrino Detector Array (AMANDA) [10], Antares [11], Nestor [12] and at Lake Baikal [13] is the search for muon neutrinos from extragalactic neutrino sources for which atmospheric neutrinos and muons present the main background.

Lepton fluxes from atmospheric charm have been calculated previously [14–17] for specific models of charm particle production. Here, we calculate the leptonic flux from charm in the context of perturbative QCD. We include next-to-leading order radiative corrections and we study the importance of the small-x behavior of the parton distribution functions. We emphasize the uncertainties inherent in the necessary extrapolation of cross sections and energy distributions beyond the experimentally measured regime. We use the comparison with low-energy charm production data to constrain some of the theoretical uncertainties, such as the charm quark mass and the factorization and renormalization scale dependence. We compare our results to the earlier work on the prompt muons from charm including a recent calculation [14] calculated using the PYTHIA Monte Carlo program [18].

In the next section, we describe the framework for the calculation of the lepton fluxes. In Sec. III, we focus on the charmed quark contribution. In Sec. IV, we present our results for the fluxes and compare with other calculations. We conclude in Sec. V.

II. LEPTON FLUX CALCULATION

Particle fluxes are determined by solving the coupled differential equations that account for production, decays, and interactions of the particles. The general form of the cascade equations describing the propagation of particle j through column depth X is given by [19,20]

$$\frac{d\phi_j}{dX} = -\frac{\phi_j}{\lambda_j} - \frac{\phi_j}{\lambda_j^{(dec)}} + \sum_k S(k \to j), \tag{2.1}$$

where λ_j is the interaction length, $\lambda_j^{(dec)} \simeq \gamma c \tau_j \rho(X)$ is the decay length, accounting for time dilation factor γ and expressed in terms of g/cm^2 units. The density of the atmosphere is $\rho(X)$ and

$$S(k \to j) = \int_E^\infty dE_k \frac{\phi_k(E_k, X)}{\lambda_k(E_k)} \frac{dn_{k\to j}(E;E_k)}{dE}. \tag{2.2}$$

In the case of production, dn/dE refers to the inclusive j production cross section $1/\sigma_k \cdot d\sigma_{k\to j}/dE$. For decays, dn/dE is the decay distribution $1/\Gamma_k \cdot d\Gamma_{k\to j}/dE$ [where $\lambda_k \to \lambda_k^{(dec)}$ in Eq. (2.2)]. Here E is the energy of the outgoing particle j.

It is possible to solve these equations numerically, however, it has been shown [14] that the same results can be obtained with an analytic solution which was derived by noticing that the energy dependence of the fluxes approximately factorizes from the X dependence. Consequently, one can rewrite

$$S(k\to j)\simeq \frac{\phi_k(E,X)}{\lambda_k(E)}\int_E^\infty dE_k \frac{\phi_k(E_k,0)}{\phi_k(E,0)}\frac{\lambda_k(E)}{\lambda_k(E_k)}\frac{dn_{k\to j}(E;E_k)}{dE}$$

$$\equiv \frac{\phi_k(E,X)}{\lambda_k(E)} Z_{kj}(E). \tag{2.3}$$

It is often convenient to write Z_{kj} in terms of an integral over $x_E \equiv E/E_k$, so

$$Z_{kj}(E)=\int_0^1 \frac{dx_E}{x_E}\frac{\phi_k(E/x_E,0)}{\phi_k(E,0)}\frac{\lambda_k(E)}{\lambda_k(E/x_E)}\frac{dn_{k\to j}(E/x_E)}{dx_E}. \tag{2.4}$$

In the limits where the flux has a single power law energy behavior, the interaction lengths are energy independent and the differential distribution is scaling (energy independent), the Z-moment $Z_{kj}(E)$ is independent of energy. In practice, the Z-moments have a weak energy dependence because dn/dx_E depends on E_k, the interaction lengths λ are not energy independent, and in general, $\phi_k(E)$ is not a constant power law in energy over the full energy range. The cosmic ray flux can be represented by the following flux of primary nucleons at $X=0$:

$$\phi_p(E,X=0)[\mathrm{cm}^{-2}\mathrm{s}^{-1}\mathrm{sr}^{-1}\mathrm{GeV}^{-1}]$$

$$=1.7\ \ (E/\mathrm{GeV})^{-2.7} E<E_0$$

$$174\ \ (E/\mathrm{GeV})^{-3}\quad E\geqslant E_0, \tag{2.5}$$

where $E_0=5\times10^6$ GeV [21,22]. At these energies, we assume isotropy of the flux [23].

The detailed solutions to the cascade equations can be found, for example, in Refs. [19] and [20]. Following Ref. [14], we assume that the incident cosmic ray flux can be represented by protons. The flux results, in high energy and low energy regimes for lepton flavor $l=\nu_\mu,\ \nu_e$, or μ due to proton production of hadron j followed by j decay into l are

$$\phi_l^{j,high}=\frac{Z_{pj}(E)Z_{jl}(E)}{1-Z_{pp}(E)}\frac{\ln(\Lambda_j/\Lambda_p)}{1-\Lambda_p/\Lambda_j}\frac{m_j c\, h_0}{E\,\tau_j}\ f(\theta)\phi_p(E,0), \tag{2.6}$$

$$\phi_l^{j,low}=\frac{Z_{pj}(E)Z_{jl}(E)}{1-Z_{pp}(E)}\phi_p(E,0), \tag{2.7}$$

where an isothermal model for the atmosphere, in which $\rho(h)=\rho_0\exp(-h/h_0)$ describes the density profile as a function of altitude h. The parameters are $h_0=6.4$ km and $\rho_0=2.03\times10^{-3}$ g/cm^3 [24]. The quantity m_j is the decaying particle's mass and

$$\Lambda_j\equiv\frac{\lambda_j}{(1-Z_{jj})} \tag{2.8}$$

is an effective interaction length, which is weakly dependent on energy. The zenith angle dependence of the high energy flux is characterized by $f(\theta)\simeq 1/\cos\theta$ for $\theta<60°$. At higher zenith angles, $f(\theta)$ is a more complicated function which accounts for the curvature of the earth. Details appear in Ref. [20]. The low energy flux is isotropic. When the cascade involves charmed hadrons, the low energy behavior dominates and the flux is called ''prompt.'' Critical energies, below which the decay length is less than the vertical depth of the atmosphere, range from $3.7-9.5\times10^7$ GeV [14]. Interpolation between high and low energy fluxes is done via

$$\phi_l=\sum_j \frac{\phi_l^{j,low}\phi_l^{j,high}}{\phi_l^{j,low}+\phi_l^{j,high}}\ . \tag{2.9}$$

Equations (2.6) and (2.7) show that the bases for the calculation of the prompt lepton fluxes are production and decay Z moments involving charm. The decay moments are discussed in Sec. III D. The main uncertainties in the calculation of the lepton flux from atmospheric charm are the production Z-moments: Z_{pD} and $Z_{p\Lambda_c}$. The production moments are given by

$$Z_{pc}=2\int_0^1\frac{dx_E}{x_E}\frac{\phi_p(E/x_E)}{\phi_p(E)}\frac{1}{\sigma_{pA}(E)}\frac{d\sigma_{pA\to c\bar{c}}(E/x_E)}{dx_E}\ , \tag{2.10}$$

where we have assumed that $d\sigma_{p\to c}/dx_E=2d\sigma_{pA\to c\bar{c}}/dx_E$. As a practical matter, we evaluate the differential cross section up to a beam energy of $E/x_E=10^{10}$ GeV. We show below that beam energies less than on the order of a factor of 10 larger than the charm energies are most relevant. The differential cross section is evaluated here using perturbative QCD. The factor of two approximates the multiplicity of charmed (or anticharmed) particles. The charm Z-moments can be converted to hadronic moments by

$$Z_{pj}(E)=f_j Z_{pc}(E)\ , \tag{2.11}$$

where f_j is the fraction of charmed particles which emerges as hadron j, where $j=D^0,\ D^+,\ D_s^+$, and Λ_c. We implicitly sum over particles and antiparticles [hence the factor of two in Eq. (2.10)].

The inelastic proton-air cross section $\sigma_{pA}(E)$ is parametrized by [25]

$$\sigma_{pA}(E)=290-8.7\ln(E/\mathrm{GeV})+1.14\ln^2(E/\mathrm{GeV})\ \ \mathrm{mb}. \tag{2.12}$$

In the high energy limit of the lepton fluxes, in addition to Z_{pc}, we need effective hadronic interaction lengths Λ_j. The proton effective interaction length is therefore

$$\Lambda_p(E)\simeq\frac{A}{N_0\sigma_{pA}(E)}\frac{1}{(1-Z_{pp})}, \tag{2.13}$$

where $A=14.5$ is the average atomic number of air nuclei and $N_0=6.022\times10^{23}$/g. We use the Thunman-Gondolo-Ingelman (TIG) energy dependent Z_{pp}, calculated using a PYTHIA Monte Carlo program [18] as a function of energy [14]. The charmed hadron j interaction lengths are all taken to be equal to the kaon interaction length, approximated by

$$\Lambda_j \simeq \frac{A}{N_0 \sigma_{pA}(E)} \frac{\sigma_{pp}^{tot}(E)}{\sigma_{Kp}^{tot}(E)} \frac{1}{(1-Z_{KK})} \ . \qquad (2.14)$$

We use Z_{KK} from Ref. [14]. The total cross sections are parametrized using the particle data book values [26] based on Regge theory [27]. The prompt lepton flux below 10^8 GeV is insensitive to the detailed values of Λ_j because essentially all of the charmed hadrons decay before reaching the surface of the earth. Therefore, for most of the energy range considered here, the charmed particles are ''low energy'' and Eq. (2.7) describes the lepton fluxes.

We now turn to the evaluation of Z_{pc} in perturbative QCD and the other charm inputs.

III. CHARM CROSS SECTION AND ENERGY DISTRIBUTION

The charm production cross section and energy distribution are the largest uncertainties in the calculation of the prompt lepton fluxes. Since the charm quark mass is of the order of 1.3 GeV, the treatment of the charm quark as a heavy quark may be questionable. Theoretical uncertainties, due to the possible range of charm quark masses, as well as the usual factorization and renormalization scale dependence need to be studied. Theoretical predictions based on perturbative QCD calculation fit the available data reasonably well in the energy range up to 800 GeV beam energy [28]. However, atmospheric lepton flux calculations require beam energies up to and beyond 10^8 GeV. The parton distribution functions are needed at very small parton momentum fraction x, outside of the measured regime [29].

In this section we will address these theoretical issues: the effect of next-to-leading order corrections on the cross section and charmed particle energy distribution; charmed quark mass dependence; factorization and renormalization scale dependence; the consequences of the small-x behavior of the parton distribution functions on the interaction Z_{pc} moment; and the A dependence of the proton-air charm production cross section.

From our evaluation of these quantities, a theoretical uncertainty associated with perturbative charm production will be evaluated. We also describe our inputs to the decay moments of charmed hadrons.

A. Total cross section

The next-to-leading order (NLO) total charm cross section has been calculated by Nason, Dawson, and Ellis [30] and by van Neerven and collaborators [31]. The NLO cross section is a factor of between 2 and 2.5 larger than the leading order cross section. Gluon fusion dominates the production process. In Fig. 1, we show the importance of the charm quark mass in the NLO cross section. We compare the NLO $\sigma(pN \to c\bar{c}X)$ as a function of the beam energy E obtained with the renormalization scale μ equal to the factorization scale M equal to the charm quark mass m_c with $m_c = 1.3$ GeV and $m_c = 1.5$ GeV. The cross sections are evaluated using the CTEQ3 parton distribution functions [32]. The

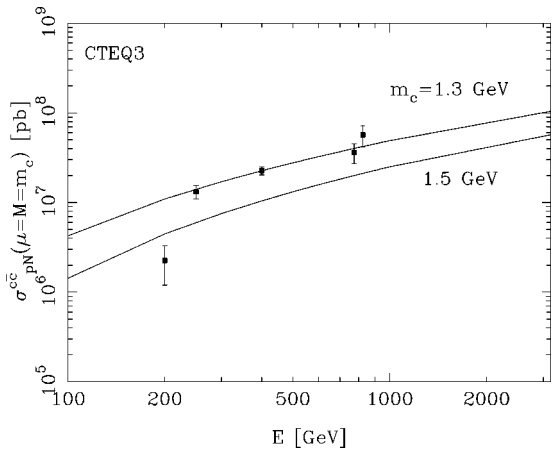

FIG. 1. The NLO $c\bar{c}$ production cross section in pN collisions versus beam energy for $m_c = 1.3$ and 1.5 GeV. The CTEQ3 parton distribution functions are used with $M = \mu = m_c$. The data are taken from the summary in Ref. [28].

corresponding value of $\Lambda_4^{\overline{MS}}$ is 239 MeV. Fixed target data from a summary by Frixione *et al.* [33] are also plotted. We note that the fixed target data seem to prefer $m_c = 1.3$ GeV. In all of the subsequent figures, we set $m_c = 1.3$ GeV. The CTEQ3 parton distribution functions will be our canonical set, in part because they incorporate global fits to the DESY ep collider HERA data, and while their validity is not claimed for parton fraction x below $x_{min} = 10^{-5}$ and $Q_0 = 1.6$ GeV, the program nevertheless provides smooth parton distribution functions which are solutions to the Altarelli-Parisi equations below these values.

In Fig. 2 we show dependence of the total cross section on the scale and parton distribution. We plot the NLO cross section for different values of μ and M: using the CTEQ3 structure functions, we set $\mu = M = m_c$ (dot-dashed) and $\mu = m_c, M = 2m_c$ (solid) with $m_c = 1.3$ GeV. The dashed line is the cross section obtained with the Martin-Roberts-Stirling

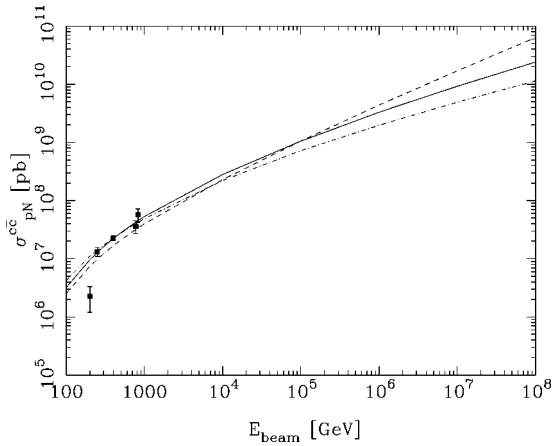

FIG. 2. A plot of NLO $\sigma_{pN}^{c\bar{c}}$ versus beam energy for $m_c = 1.3$ GeV using the CTEQ3 (solid) and D- (dashed) parton distribution functions with $M = 2m_c$ and $\mu = m_c$. Also shown is the CTEQ3 NLO prediction with $M = \mu = m_c$ (dot-dashed). The data are the same that appear in Fig. 1.

set D- (MRSD-) parton distribution functions [34] and scales $\mu = m_c, M = 2m_c$ with $m_c = 1.3$ GeV. Also plotted are the data as in Fig. 1.

The MRSD- distribution functions have a small-x behavior that is suggested by the Balitskii-Fadin-Kuraev-Lipatov (BFKL) approach [35]. In the small-x limit, the parametrization of the gluon (and sea quark) distribution functions at reference scale Q_0 is

$$xg(x,Q_0) \sim x^{-\lambda} \quad . \tag{3.1}$$

Power law extrapolations of small-x distribution functions are discussed in Ref. [36]. The D- distributions have $\lambda = 0.5$. Typically, global fits such as the MRSA [37], MRSG [38], and CTEQ3 distributions have $\lambda \simeq 0.3$. By using the D- distributions, we are effectively setting an upper limit on the perturbative charm cross section, given our choices of m_c, μ and M. We note that, generally, parton distribution functions begin evolution at Q_0 larger than 1.3 GeV. Consequently, our default factorization scale is $M = 2m_c$ so that we can use more than the CTEQ3 parametrizations.

Figure 2 indicates that at low energies, the total cross section has weak dependence on the choice of the scale and the parton distribution function. At high energies, $E \geqslant 10^6$ GeV, there is a factor of 1.7–2.1 increase from $M = m_c$ to $M = 2m_c$. The D- cross section is a factor of 1.3 larger than the CTEQ3 cross section at $E = 10^6$ GeV, both with $M = 2m_c$. The D- cross section increases more rapidly because of the steeper small-x behavior of the parton distribution function and is enhanced by a factor of 2.6 at 10^8 GeV. This gives an overall uncertainty of factor of 5.5 at the highest energy of 10^8 GeV. The MRSA and MRSG cross sections for $M = 2m_c$ lie between the upper and lower curves in Fig. 2.

The total charm cross section in p-Air collisions, $\sigma_{pA \to c\bar{c}}(E)$, can be written as

$$\sigma_{pA \to c\bar{c}} = A^{\gamma} \sigma_{pN \to c\bar{c}}. \tag{3.2}$$

We have evaluated the A dependence for charm pair production using a Glauber-Gribov model of nuclear shadowing [39]. We find that over an energy range of $10^2 - 10^6$ GeV, $\gamma = 1.0 - 0.8$. Since $A = 14.5$, the shadowing effect is small, so we set $\gamma = 1$. This is consistent with recent measurements at $E = 800$ GeV [40]. Low energy measurements at larger x_E [41] indicate smaller γ values ($\gamma \simeq 0.75$), which would reduce our flux predictions by an overall factor of 0.5.

We have used a comparison between data and theory for the total cross section to show that $m_c = 1.3$ GeV is a reasonable choice, and to estimate the range of cross sections, related to the approximate uncertainty in the flux. To evaluate Z_{pc}, we need the energy distribution of inclusive charmed particle production. In the next section, we discuss the energy distribution of charm quarks in NLO QCD.

B. Charm energy distribution

NLO single differential distributions in charm quark production have been evaluated Nason, Dawson, and Ellis [42] and incorporated into a computer program, which also calculates double differential distributions, by Mangano, Nason, and Ridolfi [43]. The program is time consuming, so we have incorporated NLO corrections to $d\sigma/dx_E$ by rescaling the leading order distribution. The x_E distributions at next-to-leading order are well fit by a K-factor rescaling which is a function of x_E, where K is defined by

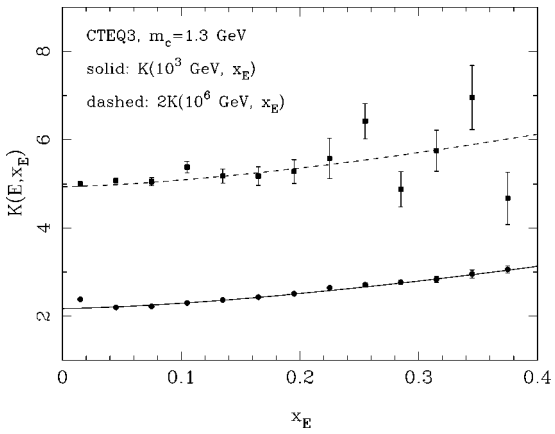

FIG. 3. The function $K(E,x_E)$ defined in Eq. (3.3) versus x_E for $E = 10^3$ GeV and 10^6 GeV. The points come from the evaluation of K using the results of Refs. [42,43] with error bars indicating numerical errors in the integration, and the curves are our fit to the ratio parametrized in Eq. (3.4).

$$K \equiv \frac{d\sigma(NLO)/dx_E}{d\sigma(``LO'')/dx_E}, \tag{3.3}$$

where ''LO'' means taking the leading order matrix element squared, but using the two-loop $\alpha_s(\mu^2)$ and the NLO parton distribution functions. K defined this way shows the effects of the NLO matrix element corrections.

Using the NLO computer program with the CTEQ3 parton distribution functions, we show our results for $K(E,x_E)$ for $E = 10^3$ and $2K(E,x_E)$ for $E = 10^6$ GeV in Fig. 3. We find that K evaluated using the D- and MRSA distributions agree well with Fig. 3. The error bars indicate the numerical errors associated with the Monte Carlo integration in the NLO program. At higher energies, the errors become larger for comparable x_E because the cross section is dominated by small x_E. K can be parametrized as

$$\begin{aligned} K(E,x_E) = {} & 1.36 + 0.42 \ln(\ln(E/\mathrm{GeV})) \\ & + (3.40 + 18.7(E/\mathrm{GeV})^{-0.43} \\ & - 0.079 \ln(E/\mathrm{GeV})) x_E^{1.5} \end{aligned} \tag{3.4}$$

for $\mu = m_c$ and $M = 2m_c$. The parametrization is shown by the curves in the figure.

Using the x_E and energy dependent K factor, we plot the charm quark x_E distribution for $E = 10^3$ GeV, 10^6 GeV, and 10^9 GeV in Fig. 4. The distributions fall rapidly with x_E. The convolution of the differential distribution with the

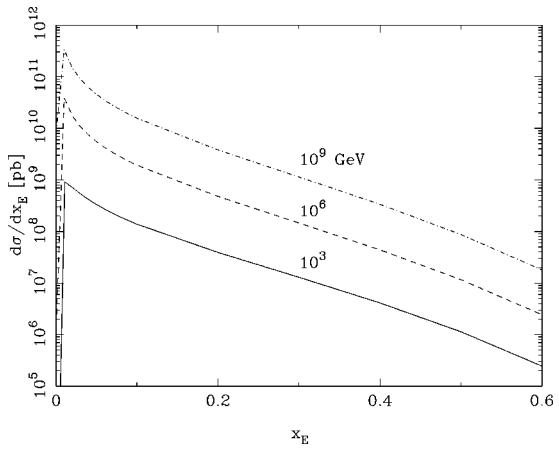

FIG. 4. For $E=10^3$ (solid), 10^6 (dashed) and 10^9 GeV (dot-dashed), $d\sigma/dx_E$, including the factor of $K(E,x_E)$. The scales used are $\mu=m_c$ and $M=2m_c$, for $m_c=1.3$ GeV.

ratio of proton fluxes and interaction lengths, integrated over x_E at fixed outgoing charm quark energy, is what is required for the *Z*-moment.

Figure 5 shows the differential moment, dZ_{pc}/dx_E. The solid lines are for CTEQ3 distributions at outgoing charm energies $E=10^4$ GeV, 10^6 GeV, and 10^8 GeV, in increasing magnitudes. The dashed lines represent the same quantities for the D- calculation. The D- distributions have approximately the same shape as the CTEQ3 distributions, but there is a more rapid growth in overall normalization with energy.

In the context of perturbative hard scattering production of charm pairs, the average x_E value in the evaluation of Z_{pc} is 0.15–0.2. More than 80% of the cross section comes from charm transverse momenta below a value of $2m_c$. In the low transverse momentum limit, $x_E \simeq x_F$. Fixed target experiments measure $d\sigma/dx_F$. The measured charmed meson x_F distributions are consistent with the perturbative NLO QCD calculations for charm quark production, without any fragmentation corrections that would soften the x_F distributions

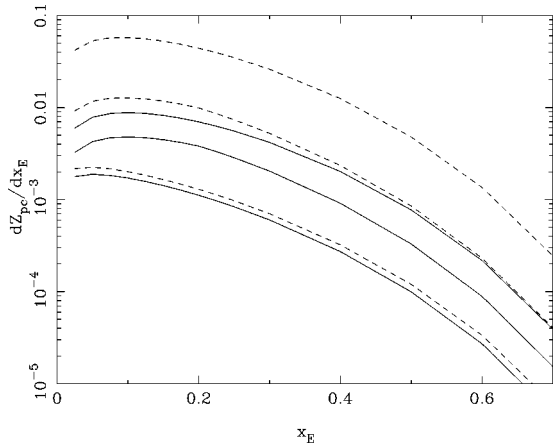

FIG. 5. For energies $E=10^4$ GeV, 10^6 GeV, and 10^8 GeV, $dZ_{pc}(E)/dx_E$ versus x_E for CTEQ3 (solid) and D- (dashed) parton distribution functions, where $\mu=m_c$ and $M=2m_c$.

[44]. Fragmentation calculations are applicable at large transverse momentum. For the calculation of Z_{pc}, we are in the low transverse momentum regime, so we do not need fragmentation.

C. Hadron fractions

We account for the transformation of charmed quarks into hadrons by an energy independent hadronic fraction. The hadronic fractions convert Z_{pc} into the interaction moments for the charmed mesons and the Λ_c via Eq. (2.11). The hadron fractions can be obtained by the observation that [33,45]

$$\sigma(D_s) \simeq 0.2\sigma(D^0+D^+), \tag{3.5}$$

$$\sigma(\Lambda_c) \simeq 0.3\sigma(D^0+D^+) \ . \tag{3.6}$$

The fractions of charmed quarks that appear as D_s and Λ_c are

$$f_{D_s}=0.13 \ , \tag{3.7}$$

$$f_{\Lambda_c}=0.20. \tag{3.8}$$

To get the D^+ and D^0 fractions, one needs a ratio of $\sigma(D^+)/\sigma(D^0)$. Using arguments based on isospin invariance and counting of states in the production of D and D^*, together with branching fractions for $D^* \to D$, Frixione *et al.* [33] suggest that $\sigma(D^+)/\sigma(D^0) \simeq 0.32$. With this assumption for the ratio of the cross sections,

$$f_{D^0}=0.51, \tag{3.9}$$

$$f_{D^+}=0.16. \tag{3.10}$$

There is some uncertainty in the values of f_j. Experimental measurements of $\sigma(D^+)/\sigma(D^0)$ in pN and pp fixed target experiments tend to lead to a somewhat higher ratio of cross sections. For example in pp collisions with a beam energy of $E_b=400$ GeV, the LEBC-EHS Collaboration [46] measures $\sigma(D^+)/\sigma(D^0)=0.7\pm0.1$, while in pN collisions at $E_b=250$ GeV, the ratio is measured by E769 [47] to be 0.57 ± 0.22. By taking $\sigma(D^+)/\sigma(D^0)=0.6$, the resulting change in the predicted flux is only $\sim 15\%$.

Integrated *Z*-moment Z_{pD^0} scaled by 10^3 versus charmed particle energy is shown in Fig. 6 for the D- and CTEQ3 distributions with $\mu=m_c$ and $M=2m_c$. Also shown is the CTEQ3 calculation with $\mu=M=m_c$. The other *Z*-moments for charm production are simple rescalings of Fig. 6. While the curves are similar up to 1 TeV, by $E=10^6$ GeV, there is a factor of ~ 5 between the upper and lower curves. At $E=10^8$ GeV, the upper and lower curves differ by more than a factor of 10, larger than the ratio of cross sections at the same energy. This is accounted for by the fact that the *Z*-moments at energy *E* involve integrals of the cross section at a higher energy. In addition, since $x_E \sim 0.15-0.2$ and the cross section is dominated by parton invariant masses near m_c, small parton *x* values are emphasized. Since the prompt flux is proportional to Z_{pc}, this enhancement is reflected in the flux as well.

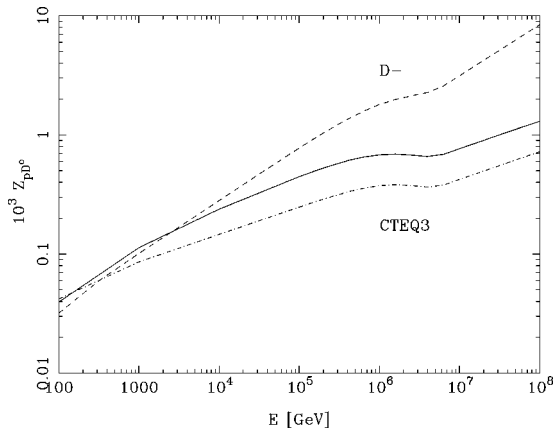

FIG. 6. $Z_{pD^0}\times 10^3$ versus E for CTEQ3 (solid) and D- (dashed) parton distribution functions with $\mu=m_c$ and $M=2m_c$. Also shown is $Z_{pD^0}\times 10^3$ for CTEQ3 with $\mu=M=m_c$ (dot-dashed).

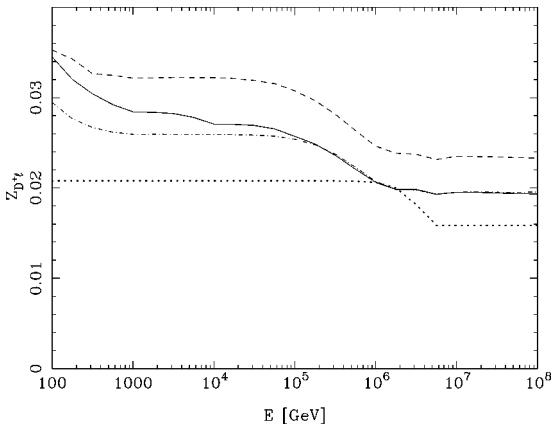

FIG. 7. The decay moment for low energy $D^+\to l$ versus energy for D- (dashed) and CTEQ3 (solid) with $M=2\mu=2m_c$ and for CTEQ3 with $M=\mu=m_c$ (dot-dashed). The dotted line indicates the decay moment if Z_{pc} is taken independent of energy.

D. Decay moments

The last elements of the calculation of the lepton fluxes from charm are the decay moments $Z_{kl}(E)$ for $k=D^+,\ D^0,\ D_s^+$, and Λ_c. The decay moments can be written in the same form as Eq. (2.4) with λ_k now representing the decay length. The decay distribution can be represented by

$$\frac{dn_{k\to l}(E;E_k)}{dE}=\frac{1}{E_k}F_{k\to l}\left(\frac{E}{E_k}\right)\ , \tag{3.11}$$

so the decay moments, in terms of an integral over $x_E=E/E_k$, are

$$Z_{kl}(E)=\int dx_E\frac{\phi_k(E/x_E)}{\phi_k(E)}F_{k\to l}(x_E)\ . \tag{3.12}$$

The function F is given in Refs. [20,17], in the approximation that the leptonic decays of charmed mesons are approximated by three-body decays. In the ultrarelativistic limit, F is nearly equal for $l=\nu_e,\ \nu_\mu$, and μ, so the decay moments for the three leptons are essentially equal. Consequently, we take the fluxes for the three leptons to be equal.

Following Bugaev *et al.* in Ref. [17], the effective hadronic invariant mass m_X of the decay of the D^+ is taken to be 630 MeV and for the D^0 decays, 670 MeV. We take $m_X=840$ MeV for D_s decays. The Λ_c will ultimately contribute little over most of the energy range considered. For Λ_c decays, we use the same three-body formula with an effective hadronic mass of 1.3 GeV. The branching ratios are

$$\begin{aligned}B(D^+\to l)&=17\%,\\ B(D^0\to l)&=6.8\%,\\ B(D_s\to l)&=5.2\%,\\ B(\Lambda_c\to l)&=4.5\%.\end{aligned} \tag{3.13}$$

For the energies considered here, the charmed particle fluxes in the low energy limit dominate. Assuming that Z_{pp} and Λ_p are nearly energy independent, this means that

$$\phi_k\sim Z_{pk}(E)\,E\phi_p(E)\ . \tag{3.14}$$

The proton flux falls like $E^{-2.7}-E^{-3}$. The charm production Z-moments increase with energy, as seen in Fig. 6. When we put in the low energy D^+ meson flux and evaluate the Z_{D^+l} moment, we get the results shown in Fig. 7. All of the other low energy decay moments can be obtained by branching fraction rescaling. For the high energy moments, we take $Z_{pk}\sim E^{0.42}$ for the D- distributions and $Z_{pk}\sim E^{0.23}$ for CTEQ3, with $\phi_k\sim Z_{pk}(E)\phi_p(E)$.

IV. PROMPT LEPTON FLUX

In Fig. 8(a) we show our results for the prompt atmospheric flux scaled by E^3 for two parton distributions and factorization scale choices. The highest flux at $E=10^8$ GeV is with the D- distributions and $M=2\mu=2m_c$ (dashed). The CTEQ3 distributions with the same choice of scale are represented by the solid line, while the dot-dashed line shows the result when $M=\mu=m_c$. For reference, we show the vertical conventional and prompt flux calculated and parametrized by TIG in Ref. [14]. The fluxes directly reflect the interaction Z-moments of Fig. 6. We emphasize that the prompt flux is isotropic except at the highest energies, while the conventional flux is not.

We have also estimated the flux due to pion-air interactions creating charm pairs. The effect is to increase the prompt flux by $\sim 30\%$ at 10^2 GeV and by $\sim 15\%$ at 10^6 GeV. This is a small effect, so we neglect pion contributions to charm production.

The prompt lepton flux evaluated using perturbative QCD can be parametrized as

$$\begin{aligned}&\log_{10}(E^3\phi_l(E)/(\mathrm{GeV}^2/\mathrm{cm}^2\ \mathrm{s}\ \mathrm{sr}))\\ &\quad=-A+Bx+Cx^2-Dx^3,\end{aligned} \tag{4.1}$$

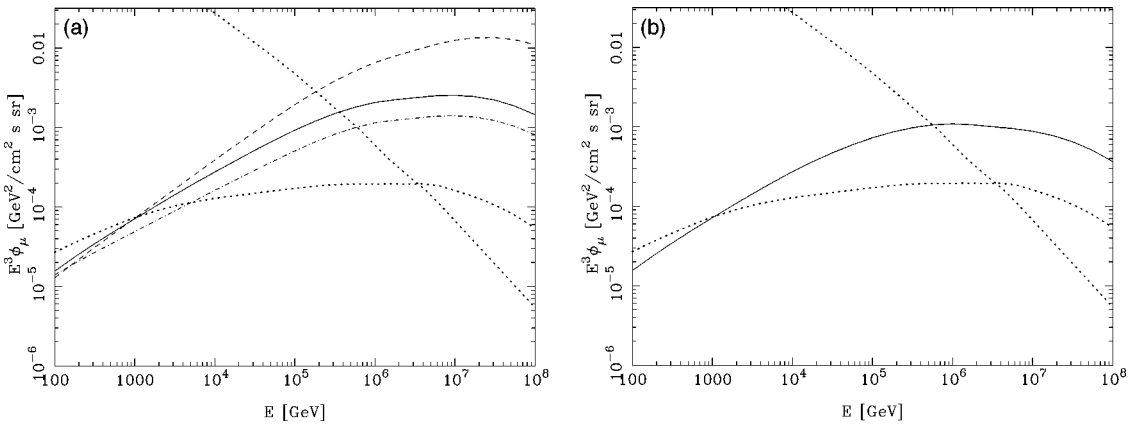

FIG. 8. (a) The prompt atmospheric muon flux scaled by E^3 versus muon energy for CTEQ3 (solid) and D- (dashed) with $M=2\mu=2m_c$. Also shown is the scaled muon flux using CTEQ3 with $M=\mu=m_c$ (dot-dashed) and the TIG parametrization of the prompt muon flux and the vertical conventional muon flux (dotted). (b) The dotted lines as in (a), and our calculation of the prompt muon flux assuming a flattening of the parton distribution functions below $x_c=10^{-4}$ according to Eq. (4.2).

where $x\equiv\log_{10}(E/\mathrm{GeV})$. In Table I, we collect the constants for the D- and CTEQ3 fluxes exhibited in Fig. 8(a).

The TIG flux relies on PYTHIA calculations with $m_c=1.35$ GeV and the MRSG [38] parton distribution functions. For $E<1$ TeV, the TIG flux is larger than ours because of fragmentation effects. Their calculation uses the Lund hadronization model [48] which can give the charmed hadron a larger energy than the charmed quark, an effect which is larger for smaller center of mass energies. The TIG prompt flux calculation is lower than our calculation for energies $E>1$ TeV. At parton $x<10^{-4}$, the parton distributions in the TIG calculation are flattened. For example, the gluon distribution is

$$xg(x,Q)\sim x^{-0.08} \tag{4.2}$$

below $x=10^{-4}$. NLO effects in the TIG calculation are accounted for by an energy and x_E independent factor of 2. Overall, the net effect is that the TIG Z_{pc} is nearly energy independent.

We note that HERA data [29] show no indication of flattening in the measured range, for example, for $3\times10^{-5}<x$ and $Q^2\sim2$ GeV^2. However, at some critical value $x<x_c$, the growth of the parton distributions at small x must slow. If the sea quark and gluon distribution functions are flattened according to Eq. (4.2) with $x_c=10^{-6}$, the flux is $\sim70\%$ of the value shown by the solid curve in Fig. 8(a) at $E=10^8$ GeV. For $x_c=10^{-5}$, the calculated prompt flux at $E=10^6$ GeV is $\sim80\%$ of the solid curve in Fig. 8(a), reducing to $\sim40\%$ of the value at 10^8 GeV. For comparison with TIG, we show in Fig. 8(b) our evaluation of the prompt neutrino flux using CTEQ3 with $M=2\mu=2m_c$, flattened according to Eq. (4.2) below $x_c=10^{-4}$. Our results are a factor of 6–7 higher than the TIG results. The discrepancy between the two calculations appears to be due to the inclusion of hadronization in PYTHIA.

TABLE I. Parameters for the prompt muon plus antimuon flux appearing in Fig. 8(a): $\log_{10}(E^3\phi_\mu/(\mathrm{GeV}^2/\mathrm{cm}^2\ \mathrm{s\ sr}))=-A+B\,x+C\,x^2-D\,x^3$, where $x\equiv\log_{10}(E/\mathrm{GeV})$.

PDF	Scales	A	B	C	D
CTEQ3	$M=\mu=m_c$	5.37	0.0191	0.156	0.0153
CTEQ3	$M=2\mu=2m_c$	5.79	0.345	0.105	0.0127
D-	$M=2\mu=2m_c$	5.91	0.290	0.143	0.0147

The prompt muon flux evaluated by Volkova *et al.* [16] is larger than our calculated flux. This comes in part because of their assumption that $d\sigma/dx_E\sim(1-x_E)^5/x_E$, independent of center of mass energy and a cross section larger than the perturbative one below $E\sim10^5$ GeV. This x_E dependence is harder than the perturbative x_E dependence shown in Fig. 4.

Bugaev *et al.* [17] have presented calculations of the prompt muon flux using two phenomenological, nonperturbative approaches. One is based on the recombination quark-parton model (RQPM) and the other on the quark-gluon string model (QGSM). The QGSM prompt flux is relatively small compared to the RQPM flux, which already affects the total atmospheric muon flux at energies of a few tens of TeV. Relative to the RQPM calculation and the Volkova *et al.* results, our D- prompt flux is lower.

Several experiments show an excess in muon flux above ~10 TeV [7–9]. Following Rhode in Ref. [7], we plot in Fig. 9 the quantity $E^{3.65}\phi_\mu(E)$, where ϕ_μ represents the sum of the prompt and vertical conventional flux. Also shown are the data from Ref. [7]. The energy scale factor mostly accounts for the rapidly falling conventional flux [49]. When we add the prompt fluxes of Fig. 8(a) to the TIG vertical conventional flux, one sees an enhancement at muon energies above 10^5 GeV, at a higher energy than the experimental excess shown by data points.

In Ref. [50], we have shown that it is possible to enhance the prompt flux sufficiently to account for some of the observed muon excess at a few TeV. This is accomplished by extrapolating the charm cross section at 1 TeV with a faster growth in energy than predicted by perturbative QCD. The x_E dependence was taken as $d\sigma/dx_E\sim(1-x_E)^4$. The inputs are consistent with fixed target data below 1 TeV beam energies. We found that the predicted prompt flux made sig-

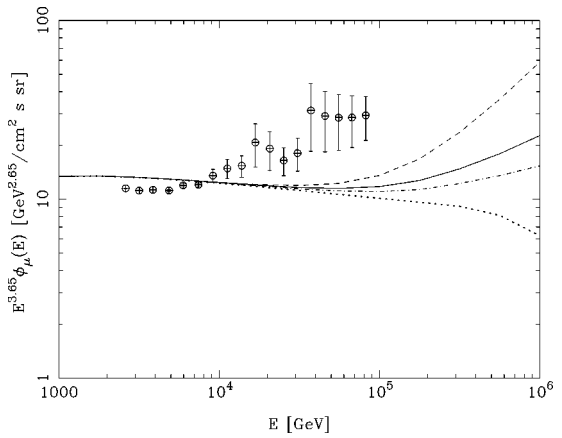

FIG. 9. The prompt plus vertical conventional atmospheric muon flux scaled by $E^{3.65}$ versus muon energy for CTEQ3 (solid) and D- (dashed) with $M=2\mu=2m_c$. Also shown is the scaled muon flux using CTEQ3 with $M=\mu=m_c$ (dot-dashed) and the TIG parametrization of vertical conventional muon flux (dotted). The data shown are from Ref. [7].

nificant contributions in the region of the observed excess of muons, but it does not fully describe the Fréjus data [7]. These inputs are not consistent with perturbative QCD. The experimental excess of muons cannot be accounted for by perturbative QCD production of charm.

Another implication of the prompt fluxes calculated here is the ratio of the muon neutrino to electron neutrino flux. We define

$$R_\theta=\frac{\phi_{\nu_\mu}}{\phi_{\nu_e}} \ . \tag{4.3}$$

Using the TIG parametrization of the vertical $\theta=0°$ neutrino fluxes, adding conventional and prompt contributions, R_0 as a function of energy is shown in Fig. 10. At a zenith angle of 60°, the conventional flux is a factor of two larger. The ratio R_{60} is also shown in Fig. 10. The quantity R is an interesting

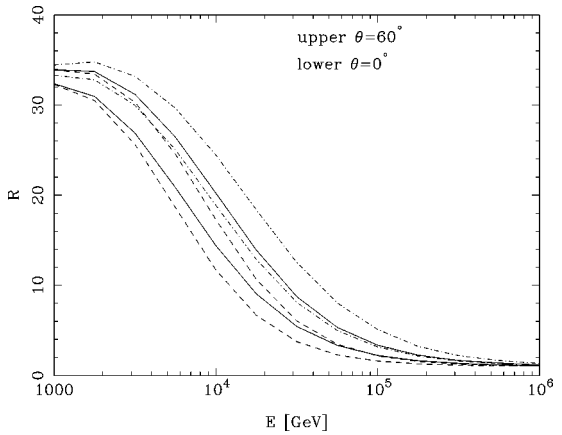

FIG. 10. $R=\phi_{\nu_\mu}/\phi_{\nu_e}$ for zenith angles 0° and 60° versus neutrino energy for CTEQ3 (solid) and D- (dashed) with $M=2\mu=2m_c$, and using CTEQ3 with $M=\mu=m_c$ (dot-dashed).

diagnostic for the onset of prompt neutrino dominance. Unfortunately, at these energies, R is difficult to measure.

V. CONCLUSIONS

We find that the perturbative charm contributions to lepton fluxes are significantly larger than the recent TIG calculation. The prompt muon flux becomes larger than the conventional muon flux from pion and kaon decays at energies above $\sim 10^5$ GeV. We set values of the charmed quark mass, renormalization scale and factorization scale by fitting the charm production cross section to low-energy data. Using these values, we extrapolate the inclusive charm energy distribution to higher energies. We have evaluated the energy distribution at NLO in QCD, and we find that the NLO corrections give a correction of more than a factor of two which is weakly energy and x_E dependent. Nuclear shadowing corrections are small for all energies, due to the air nucleus being relatively light.

The main uncertainty in the perturbative calculation of the prompt flux, given fixed charm mass, factorization scale and renormalization scale, is the small-x behavior of the parton distribution functions. The spread in predictions at $E=10^8$ GeV is indicative of this uncertainty. Different choices of scales and distribution functions, extrapolated to low x with the same power law dependence as for $x>10^{-5}$, yield as much as a factor of ~ 10 discrepancy in the prompt flux at $E=10^8$ GeV. The growth of the $c\bar{c}$ cross section with energy as seen in Fig. 2 requires that the parton distribution functions must eventually slow in their growth with small parton x, however, there are no experimental indications as to where this should begin, given $Q=m_c-2m_c$. An abrupt turnover in the power law behavior of the small-x parton distributions is unlikely. Even with an abrupt onset of small-x flattening of the parton distribution functions at $x_c=10^{-4}$, our prompt fluxes are larger than TIG's calculation using PYTHIA.

We conclude that the prompt muon flux calculated in the context of perturbative QCD cannot explain the observed excess of muons in the TeV region [7–9], independent of the theoretical uncertainties associated with small parton x. However, prompt fluxes calculated using nonperturbative models of charm production such as discussed in Refs. [17,50] could provide a muon excess in that energy range. Measurements of the atmospheric flux in the 100 TeV range would help pin down the charm cross section at energies above those currently accessible using accelerators and would provide valuable information about the small-x behavior of the gluon distribution function.

Even though the prompt contributions to the lepton fluxes change the energy behavior of the differential fluxes by a factor of E, the atmospheric neutrino fluxes do not compete with neutrino fluxes from extragalactic sources above 10 TeV [51]. Possible oscillations of muon neutrinos as indicated by the Super-Kamiokande experiment [5] do not affect our results due to the extremely small oscillation probability for the energies of interest.

ACKNOWLEDGMENTS

This work was supported in part by National Science Foundation Grant No. PHY-9507688 and D.O.E. Contract No. DE-FG02-95ER40906. M.H.R. acknowledges the hospitality of the CERN Theory Division where part of this work was completed. We thank P. Gondolo, P. Nason, W. Rhode, D. Seckel, and M. Mangano for useful discussions, the Aspen Center for Physics, and M. Mangano for providing a copy of the Mangano-Nason-Ridolfi NLO computer program.

[1] For a review, see T. K. Gaisser, in *Neutrino '96*, Proceedings of the 17th International Conference on Neutrino Physics and Astrophysics, edited by K. Enquist, K. Huitu, and J. Maalampi (World Scientific, Singapore, 1997), p. 211, and references therein.

[2] R. Becker-Szendy *et al.*, Phys. Rev. D **46**, 3720 (1992).

[3] Kamiokande Collaboration, H. S. Hirata *et al.*, Phys. Lett. B **205**, 416 (1988); **280**, 146 (1992); Y. Fukuda *et al.*, *ibid.* **335**, 237 (1994).

[4] Soudan Collaboration, W. W. Allison, *et al.*, Phys. Lett. B **391**, 491 (1997); M. C. Goodman, in *Proceedings of the 25th International Cosmic Ray Conference*, 1997 edited by M. S. Potieger, B. C. Raubenheimer, and D. J. van der Walt, Vol. **7**, p. 77.

[5] SuperKamiokande Collaboration, J. G. Learned, in *Proceedings of the 25th International Cosmic Ray Conference* [4], p. 73.

[6] T. K. Gaisser, F. Halzen, and T. Stanev, Phys. Rep. **258**, 173 (1995).

[7] W. Rhode, Nucl. Phys. B (Proc. Suppl.) **35**, 250 (1994).

[8] V. N. Bakatanov *et al.*, Sov. J. Nucl. Phys. **55**, 1169 (1992).

[9] For a summary of experimental results, see E. V. Bugaev *et al.*, Phys. Rev. D **58**, 054 001 (1998), and references therein.

[10] See, for example, F. Halzen, eprint archive astro-ph/9707289. The experiment homepage is http://amanda.berkeley.edu/.

[11] Homepage http://infodan.in2p3.fr/antares/saclay/home.html.

[12] E. G. Anassontzis *et al.*, presented at the XVI International Workshop on Weak Interactions and Neutrino 97 Conference (Capri). Article available at the experiment homepage http://www.rama1.infn.it/nestor/nestor.html.

[13] Baikal Collaboration, I. Sokalski, in *Proceedings of the International Workshop XXXIInd Rencontres de Moriond–Very High Energy Phenomena in the Universe*, edited by Y. Giraud-Herand and J. Tran Thanh Van (Editions, Frontières, Gif-Sur-Yvette, 1997), p. 261. Homepage http://www.ifh.de/baikal/baikalhome.html.

[14] M. Thunman, P. Gondolo, and G. Ingelman, Astropart. Phys. **5**, 309 (1996).

[15] L. V. Volkova, Yad. Fiz. **31**, 1510 (1980) [Sov. J. Nucl. Phys. **31**, 784 (1980)]; K. Mitsui, Y. Minorikawa, and H. Komori, Nuovo Cimento C **9**, 995 (1986); A. V. Butkevich, L. G. Dedenko, and I. M. Zheleznykh, Yad. Fiz. **50**, 142 (1989) [Sov. J. Nucl. Phys. **50**, 90 (1990)]; V. Agrawal, T. K. Gaisser, P. Lipari, and T. Stanev, Phys. Rev. D **53**, 1314 (1996); L. V. Volkova and G. T. Zatsepin, Yad. Fiz. **37**, 353 (1983); H. Inazawa and K. Kobayakawa, Prog. Theor. Phys. **69**, 1195 (1983); G. Battistoni *et al.*, Astropart. Phys. **4**, 351 (1996).

[16] L. V. Volkova, W. Fulgione, P. Galeotti, and O. Saavedra, Nuovo Cimento C **10**, 465 (1987).

[17] Bugaev *et al.* [9]; E. V. Bugaev *et al.*, Nuovo Cimento C **12**, 41 (1989).

[18] T. Sjöstrand, Comput. Phys. Commun. **82**, 74 (1994).

[19] T. K. Gaisser, *Cosmic Rays and Particle Physics* (Cambridge University Press, New York, 1990).

[20] P. Lipari, Astropart. Phys. **1**, 195 (1993).

[21] P. Pal and D. P. Bhattarcharyya, Nuovo Cimento C **15**, 401 (1992).

[22] JACEE Collaboration, T. H. Burnett *et al.*, Astrophys. J. Lett. **349**, L25 (1990).

[23] A. Gregory and R. W. Clay, in *CRC Handbook of Chemistry and Physics* (CRC Press Inc., Boca Raton, FL, 1982-1983), p. F-175.

[24] K. Maeda, Fortschr. Phys. **21**, 113 (1973).

[25] H. H. Mielke, M. Foller, J. Engler, and J. Knapp, J. Phys. G **20**, 637 (1994).

[26] Particle Data Group, R. M. Barnett *et al.*, Phys. Rev. D **54**, 1 (1996), Table 36.2.

[27] A. Donnachie and P. V. Landshoff, Phys. Lett. B **296**, 227 (1992).

[28] The data were taken from a summary by S. Frixione *et al.*, in *Heavy Flavors II*, edited by A. J. Buras and M. Lindner (World Scientific, Singapore, 1995), hep-ph/9702287.

[29] H1 Collaboration, C. Adeloff *et al.*, Nucl. Phys. **B497**, 3 (1997); ZEUS Collaboration, M. Derrick *et al.*, Z. Phys. C **72**, 399 (1996).

[30] P. Nason, S. Dawson, and R. K. Ellis, Nucl. Phys. **B303**, 607 (1988).

[31] W. Beenakker, H. Kuijf, W. L. van Neerven, and J. Smith, Phys. Rev. D **40**, 54 (1989); T. Matsuura, S. C. van der Marck, and W. L. van Neerven, Nucl. Phys. **B319**, 570 (1989).

[32] CTEQ Collaboration, H. Lai *et al.*, Phys. Rev. D **51**, 4763 (1995).

[33] S. Frixione, M. L. Mangano, P. Nason, and G. Ridolfi, Nucl. Phys. **B431**, 453 (1994). See also the review by Frixione *et al.* [28].

[34] A. D. Martin, W. J. Stirling, and R. G. Roberts, Phys. Lett. B **306**, 145 (1993).

[35] E. A. Kuraev, L. N. Lipatov, and V. S. Fadin, Zh. Éksp. Teor. Fiz. **71**, 840 (1976) [Sov. Phys. JETP **44**, 443 (1976)].

[36] R. K. Ellis, Z. Kunszt, and E. M. Levin, Nucl. Phys. **B420**, 517 (1994).

[37] A. D. Martin, W. J. Stirling, and R. G. Roberts, Phys. Rev. D **50**, 6734 (1994).

[38] A. D. Martin, W. J. Stirling, and R. G. Roberts, Phys. Lett. B **354**, 155 (1995).

[39] I. Sarcevic and P. Valerio, Phys. Rev. C **51**, 1433 (1995).

[40] E789 Collaboration, M. J. Leitch *et al.*, Phys. Rev. Lett. **72**, 2542 (1994).
[41] M. E. Duffy *et al.*, Phys. Rev. Lett. **55**, 1816 (1985).
[42] P. Nason, S. Dawson, and R. K. Ellis, Nucl. Phys. **B327**, 49 (1989); **B335**, 260 (1990).
[43] M. Mangano, P. Nason, and G. Ridolfi, Nucl. Phys. **B373**, 295 (1992).
[44] See, for example, E769 Collaboration, G. Alves *et al.*, Phys. Rev. Lett. **77**, 2392 (1996).
[45] WA75 Collaboration, S. Aoki *et al.*, Prog. Theor. Phys. **87**, 1305 (1992).
[46] LEBC-EHS Collaboration, M. Aguilar-Benitez *et al.*, Z. Phys. C **40**, 321 (1988).
[47] E769 Collaboration, G. A. Alves *et al.*, Phys. Rev. Lett. **77**, 2388 (1996).
[48] T. Sjöstrand, Comput. Phys. Commun. **27**, 243 (1982).
[49] A better choice of rescaling given our assumed cosmic ray flux would be $E^{3.7}\phi_\mu$.
[50] L. Pasquali, M. H. Reno, and I. Sarcevic, Astropart. Phys. **9**, 193 (1998).
[51] For a discussion of recent models and event rates, see R. Gandhi, C. Quigg, M. H. Reno, and I. Sarcevic, Astropart. Phys. **5**, 81 (1996); Phys. Rev. D **58**, 093 009 (1998).